Insights Into Volcanic Unrest by Correlating Petrological and Seismic Observations at Kizimen (Kamchatka, Russia)

Lea Ostorero (ostorero@ipgp.fr)
Université de Paris, Institut de physique du globe de Paris, CNRS https://orcid.org/0000-0002-8279-6596

Hélène Balcone-Boissard
Institut des Sciences de la Terre de Paris (ISTeP), UMR 7193, CNRS-Sorbonne Université

Georges Boudon
Institut de Physique du Globe de Paris

Nikolai Shapiro
Institut de Sciences de la Terre https://orcid.org/0000-0002-0144-723X

Alexander Belousov
Institute of Volcanology and Seismology, 9 Piip Boulevard https://orcid.org/0000-0003-1379-9256

Marina Belousova
Institute of Volcanology and Seismology, 9 Piip Boulevard

Andreas Auer
Department of Geoscience, Shimane University, 1060 Nishikawatsu

Sergey Senyukov
Kamchatka Branch of the Geophysical Service, Russian Academy of Sciences https://orcid.org/0000-0002-7378-9095

Svetlana Droznina
Kamchatka Branch of the Geophysical Survey, Russian Academy of Sciences, 9 Piip Boulevard

Article

Keywords:

Posted Date: March 10th, 2022

DOI: https://doi.org/10.21203/rs.3.rs-1140681/v1

Version of Record: A version of this preprint was published at Communications Earth & Environment on November 19th, 2022. See the published version at https://doi.org/10.1038/s43247-022-00622-3.

Abstract

The increase of number and intensity of earthquakes during a pre-eruptive crisis is the main basis of seismic volcano monitoring. However, the exact relationship between the seismic activity and the volcano-magmatic processes remains unclear. Here we present a direct comparison between characteristics of a seismo-volcanic crisis recorded prior to the 2010-2013 eruption of Kizimen volcano (Kamchatka, Russia) and the timescales of processes in the magma plumbing system. These timescales are inferred from the modelling of Fe-Mg intracrystalline interdiffusion in 88 zoned orthopyroxene crystals from dacites and silica-rich andesites samples collected after the eruption. We show that the eruptible magmas were assembled rapidly during a magma mixing episode ~1.5 years before the eruption, which is well correlated with the onset of a seismic crisis. We conclude that the observed seismic re-activation marks the onset of magma mixing leading to destabilization of the reservoir followed by the eruption after ~1.5 years.

Introduction

During volcanic unrest the information about the magmatic processes eventually leading to an eruption can be obtained from geochemical, geodetic, and seismic observations[1–4]. The latter are particularly valuable because of their depth and time resolution. An increasing number and intensity of volcanic earthquakes is considered the hallmark of an impending eruption[5]. While the correlation between the preparation of eruptions and the increased seismic activity is well established empirically, relating the latter to specific magmatic processes remains problematic. At the same time, temporal evolution of magmatic processes in the plumbing system can be deciphered based on modern petrological and geochemical methods[6–9]. Therefore, a more direct link between seismicity and magmatic process can be obtained by comparing petrological to seismological records.

Within a reservoir, crystals grow from melt incorporating major and trace elements following thermodynamic and kinetic laws[10]. In silica-rich melt, orthopyroxenes $(Mg,Fe)_2Si_2O_6$ are relevant candidates as their composition evolve from Mg-rich to Fe-rich composition, depending especially on melt temperature and composition, creating zoned crystals[6]. Diffusion in the zoned crystals is a time-dependent process (Fick's law) acting as a clock for measuring timescales of a variety of magmatic processes[7,8,11,12]. Such zoned orthopyroxenes (opx) in mushy zones below volcanoes are thus time capsules allowing us to constrain the pre-eruptive timescales of magmatic processes[7,8,11,12].

Timescales modelled using (Fe-Mg) interdiffusion chronometer applied to well-monitored eruptions, may be correlated to monitoring data (seismicity, changes in the gas chemistry and/or flux, deformation) and then have significant implications for volcanic eruption forecasting models[7,13–18]. Up to now only syn-eruptive investigations of magmatic processes in correlation with seismic activity have been performed for differentiated systems[17,19,20] compared to pre-eruptive correlations. To establish a temporal correlation between the magmatic processes and the seismic activity during a pre-eruptive re-activation

of a plumbing system, we selected a recent eruption of Kizimen in 2010–2013, in Kamchatka, involving differentiated magmas. This eruption occurred after several decades of quiescence and was well-monitored[21–24]. Seismic network operated by the Kamchatka Branch of the Geophysical Survey of the Russian Academy of Sciences resulted in an exceptional record of the pre-eruptive seismic re-activation. Furthermore, the petrological record in the opx crystals that is very sensitive to temperature fluctuations[19,25–28] has not been perturbed by previous volcanic activity. Therefore, this 2010–2013 Kizimen eruption provides us with a unique opportunity to study magmatic-seismic correlation and better understand the processes leading to silicic magmas. We report a good correlation between the petrological timescales and the pre-eruptive seismic monitoring 18 months prior the eruption. The petrological timescales are thus a valuable warning-clock for volcano monitoring.

Geological context and previous results about the 2010 eruption of Kizimen

The Kamchatka Volcanic Arc, in Eastern Russia, results from the subduction of the northeast corner of the Pacific plate at a rate of 8–9 cm/yr beneath the Okhotsk plate (which is connected to the North American plate)[29,30] (Fig. 1a). This arc is the most productive arc on Earth (~ 310 millions of tons of magma emitted per year from the late Pleistocene to the Holocene)[31], with more than 25 active volcanic centers. One of the largest world's clusters of subduction volcanoes, the Klyuchevskoy volcanic group are located in the northern part of the arc, in the Central Kamchatka Depression[32,33] where the largest magmatic production is recorded[21,30,34] and where the volcanoes exhibit very sustained seismic activity (Fig. 1a-b). The particularly strong volcanic activity in this region can be due to the hot mantle material brought by the around-slab-edge asthenospheric flow[35] and related crustal extension[36]. Nearly continuous occurrence of deep long-period earthquakes near the crust-mantle boundary[34,37] is likely related to the underplating of mafic magmas and widespread seismic tremors mark an active trans-crustal magmatic system connecting different volcanoes of this group[38]. At the same time, well-developed magma chambers beneath some of most active volcanoes such as Bezymianny are well documented[39].

Kizimen is located in the southern part of the Central Kamchatka Depression and his magmas might have similar origin to those from the Klyuchevskoy volcanic group. Because of the less dense coverage by seismic stations, the deep structure of the crust beneath Kizimen is not well known and the reported magmatic and seismic activity is linked to the upper crust. At the same time, existence of crustal scale magmatic system in analogy with the Klyuchevskoy volcanic group cannot be excluded. In 2010–2013, Kizimen produced its first historical magmatic eruption, emitting magma volumes of 0.4 km^3 Dense Rock Equivalent (DRE) (Fig. 1b; **Supplementary Fig. 1**). On 11 November 2010, explosive episodes generated pyroclastic density currents[21,40,41], that were then followed by the extrusion of a lava dome which gradually formed a very thick lava flow (~ 200-m-thick)[41] (Fig. 1b; **Supplementary Fig. 1**). Numerous pyroclastic density currents of block and ash type were produced as a result of the gravity collapse of the lava dome and flow front emitting dacites, silica-rich andesites and banded lavas, formed by an incomplete magma mixing event between two magmas[41] (Fig. 1b-f; **Supplementary Fig. 1 and**

Supplementary Table 1). For this eruption, a model of the pre-eruptive dynamics proposed that the emitted dacitic came from the differentiation of a basaltic magma[41]. This basaltic magma was not erupted at the surface[41]. Several models have assessed the presence of a stable silicic reservoir under Kizimen, periodically refilled by magmatic injections[40–42]. This silicic magma chamber is located between 5–11 km depth (based on earthquakes depths and amphibole and opx compositions[41], which is in agreement with a study on older eruptions from Kizimen with storage pressures of magmas between 1 to 3 kbars (up to 10 km depth)[40,42]). Another seismic zone from the ground surface to ~ 5 km has been recognized during the 2010–2013 eruption and probably shows the conduit in which silicic magma ascended to the surface[41]. A mafic recharge occurred in 1963, simultaneously with a seismic crisis[21,41] and led to magma hybridization of the lower part of the dacitic reservoir, forming an andesitic magma at the base of the magmatic reservoir[41]. A large portion of the dacitic magma was not affected by this mafic recharge, leading to the formation of a zoned reservoir. Prior to the eruption of 2010, another mixing event occurred between the andesitic magma and the dacitic magma due to some degassing of this latter leading to magma convection, with incomplete mixing between the two magmas[41].

A seismic crisis started ~ 1.5 years before the eruption with earthquakes located between 11 km and the surface[21,22,41]. In addition, deformation of the volcanic edifice was detected by Interferometric synthetic aperture radar (InSAR)[23]. The seismic data and deformation by InSAR were interpreted as the injection of a dyke of 15 km length and 15 cm thickness in the magmatic reservoir[23]. But, as no seismicity below 12 km has been recorded, this interpretation is thought not to fit the existing geological and seismological data[41]. Kizimen is crossed by an active tectonic fault, through which volatiles are escaping to the surface. This leakage is visible as a persistent fumarole on the NW flank of the volcano[41], this long-term passive degassing could be responsible for the depressurization of the magma chamber and increase the viscosity of the magma[43,44] (Fig. 1b). This high viscosity of the silicic magma feeding system could prevent the intermixing between the silicic magma and ascending magmas from depth, that could be responsible for the long repose time periods between the input of magma from depth in 1963 and the following eruptions[41]. The temperatures of the fumaroles at the summit of Kizimen have been measured from 15–31 August 2009 and a temperature of 340°C was reached close to the central mouth of the outermost fumaroles on Kizimen which is higher than measurements prior to the onset of the unrest (maximum of ~ 270°C)[45]. However, this temperature increase of the fumaroles is not thought to be a consequence of seismic activation[45]. One month before the eruption, visual signs of reactivation were observed with thermal areas and two new large fumaroles that appeared (16 October 2010)[21,41].

Results

Magmas are differentiated, with whole rock compositions in the andesitic and dacitic field (Fig. 1c-d; **Supplementary Note and Supplementary Table 1**). Opx are present in the dacite and andesite. 70% are unzoned (**Supplementary Fig. 2**). Zoned crystals were classified according to the type of zonation observed: either a single one (normal or reverse zonation) or a multiple one (Fig. 1g-j; **Supplementary**

Fig. 2). In the dacite, the majority of opx are normal-zoned while, in the andesite, reverse-zoned opx are more abundant (**Supplementary Fig. 2**). Few opx show reactional borders or remelting textures (**Supplementary Fig. 2**). Out of the 1832 opx crystals mounted, 112 zoned opx compositions and 108 unzoned opx compositions were investigated in the dacite and andesite (**Supplementary Data 1)**. Opx compositions are spread over an En_{44-73} compositional range (Enstatite content ($En = \frac{Mg}{Mg+Fe}$)), with three compositional groups identified *(*En_{62-64}: all cores (unzoned and zoned opx), En_{44-54}: normal-zoned rims of the dacite, En_{64-73} reverse-zoned rims in the andesite*)* (**Supplementary Fig. 3 and Supplementary Data 1**).

Timescales

Of 112 profiles on zoned crystals, 26 were suitable for diffusion modelling for the dacite, as well as 62 for the andesite. The temperatures used to model the timescales are calculated on magnetite/ilmenite couples in the dacite and andesite, this equilibrium between these minerals has been widely used to estimate temperatures in igneous rocks[46]. Mean temperature of 832 ± 37°C and 847 ± 57°C are found for the andesite and dacite respectively[46] (**Supplementary Note, Supplementary Fig. 4 and Supplementary Data 2–3**). These profiles have sigmoidal shapes due to diffusion effects, without bumps or peaks that could indicate a growth component[25]. Al_2O_3 and CaO gradients are also compared to the En content to verify that the gradients in En are due to diffusion[47] (**Supplementary Fig. 5**; **Supplementary Data 1**). For both the dacite and andesite, 80% of the timescales are in the 1.5-years period prior to the eruption whatever the type of zoning (normal or reverse) (Fig. 2b **and d; Supplementary Figs. 4 and 6 and Supplementary Data 3**).

Discussion

Interdiffusion timescales modelling of the zonations in the opx help us to retrieve the timescales of magmatic processes that modify the storage conditions before volcanic eruptions (changes in temperature, pressure, oxygen fugacity (fO_2) or volatile content)[13,15,25,48,49] (Fig. 2b **and d**; **Supplementary Fig. 4**).

As 70% of the opx are unzoned, this suggests that the magmatic changes did not affect the entire magmatic reservoir. All the opx have the same core compositions (**Supplementary Fig. 3 and Supplementary Data 1**), meaning that the opx from the dacite and the andesite originated from the dacitic magma present in the reservoir before the 1963 basaltic injection. The andesitic part of the reservoir was then formed in 1963 after the injection of an aphyric basaltic magma and mixed with the dacite in the lower part of the reservoir, as suggested in a previous study of the eruption[41]. This is confirmed by previous study for plagioclase crystals in banded rocks of the same eruption[41]. No zoned opx studied reflected this longer timescale (~ 47 years) (**Supplementary Fig. 4**). 1.5 years prior to the eruption of 2010, after ~ 47 years of dormancy, the opx in the dacitic and andesitic magmas record a magmatic reactivation accompanied by changes in the storage conditions in their respective storage

areas, with different processes as their most external zonations are not the same (Fig. 2b **and d; Supplementary Fig. 2**). Reverse zonations in the andesite reflect heating processes, by a magma injection or magma mixing[17,25]. These events probably generated an overpressure in the reservoir at the origin of the seismicity recorded during the same time period (Fig. 2a-d), April 2009-November 2010. On the contrary, normal zonations for the dacite register degassing or cooling processes[15,17,25] (Fig. 3a). As the temperature of the andesitic part below the dacite would increase, following mixing with other parts of the reservoir, the dacitic reservoir is unlikely to cool down. But this magma mixing episode in the andesitic reservoir[15] may have led to fluid saturation and volatile degassing in the dacitic part of the reservoir that may have generated the normal zonations in the dacite (Fig. 3a). Indeed, a strong and persistent fumarole is present on the NW flank of Kizimen, showing the degassing of the reservoir. This long-term passive degassing is thought to depressurize the magma chamber and increase the viscosity of magma in the shallow chamber[41]. Another scenario could consist in an aphyric mafic injection (as no opx have a different En core composition) leading to the same zonations in opx as in the first scenario. But as no deep earthquakes (> 11 km) have preceded and accompanied the 2010 eruption, this event is not likely to have been triggered by input of basic magma from greater depth[41]. Furthermore, no enclaves of basaltic or basaltic andesite compositions were found, unlike many of the earlier eruption products[40]. Magma mixing is then the preferred process to interpret the zonations in the opx. Finally, magma mingling occurred between the andesitic and dacitic lower parts, during the magma ascent, forming the banded andesites and dacites, along with the increase of the number of earthquakes recorded (Fig. 2; Fig. 3b) up to the eruption on 11 November 2010.

80% of the modelled timescales cover the period between April 2009 and the onset of the eruption on 11 November 2010 and 60% from January 2010 to November 2010 (Fig. 2b **and d**). The uncertainties associated to the timescales modelled are mainly due to the temperature uncertainty and uncertainties due to diffusion coefficient determination[6,25,50] (see Methods). For most of the short timescales (< 2 years), the positive error associated to the timescale is in the order of 1 year and the negative error is around 100 days (**Supplementary Fig. 4; Supplementary Data 3**). The temperatures used to model the timescales determined in the magnetite/ilmenite pairs can show the variability of the temperatures sampled in the reservoir. Varying the temperature and using the one determined in opx in the andesitic part of mingled samples by another study[41] implies shorter timescales for the andesite (divided by 2, with T = 875°C), showing the importance of the choice of the temperature in the timescale modelling. As no temperature was determined in opx of the dacite in the previous study[41] and no melt inclusion with a sufficient size was found in our samples, the temperatures determined on the magnetite/ilmenite pairs were used.

The distribution of timescales obtained on the opx crystals can be correlated with the seismic activity (Fig. 2). For this goal, we used the catalog of volcanic earthquakes produced by the Kamchatkan Branch of Russian Geophysical Service. The completeness magnitude for this catalog is difficult to estimate and can be variable in time depending on the number of stations and meteorological conditions. Therefore, instead of reporting the number of recorded earthquakes (that is strongly sensitive to this completeness

magnitude) we use the cumulative seismic moment that is dominated by strongest earthquakes (Fig. 2a-d). Also, this quantity is closely related to the overall energy seismic release and therefore has a physical relationship with ongoing processes within volcano. Because Kizimen remained quiescent for decades and is located far from other volcanoes, this catalog is exclusively related to the 2010 eruption. The increase in number of petrological timescales coincides with the onset of the seismic crisis recorded ~ 1.5 years before the eruption[21,41], with earthquakes between ~ 3 to 13 km from April 2009 to January 2010 and then becoming more numerous and shallower from January 2010 to the eruption (Fig. 2a **and c**, **Supplementary Fig. 6**). We note that the apparent migration of the seismicity around January 2010 becoming shallower (Fig. 2a **and c**), between − 5 km to + 3 km is likely due to the modification of the software used for the analysis of the earthquakes[21]. While this modification might affect the number of detected small earthquakes its influence on the cumulative seismic moment is negligible (Fig. 2b **and d)**. Ground deformation was also detected before the eruption, from September 2008 to September 2010 (InSAR data)[23]. These types of signals are due to magma transfers below the volcano before the eruption[13,14]. The increase of temperatures of the fumaroles measured in August 2009[45], are compatible with the degassing at depth in the reservoir (Fig. 3).

The opx chronometer is thus successfully used here to determine the links between pre-eruptive magma dynamics in the plumbing system and pre-eruptive monitoring data at the surface for an eruption involving differentiated magma. This chronometer shows the reactivation of the magmatic feeding system of Kizimen 1.5 years before the eruption, well correlated with the monitoring signals recorded on the surface from April 2009 to the time of eruption. Most of the studies investigating petrology and monitoring signals are carried out in mafic systems, using olivines, such as Mt Etna (Italy)[13,15], Kilauea (Hawai'i)[51], Eyjafjallajökull (Iceland)[14], Piton de la Fournaise (La Réunion)[52] and El Hierro (Canary Islands)[2,53], Shishaldin volcano (Alaska)[16] or Llaima (Chile)[54]. Only three studies have used opx chronometer, but to investigate syn-eruptive monitoring[17,19,20]. On Mount St-Helens correlations were made with some eruptive phases during the 1980 eruption but no correlation was made with seismicity before the beginning of the eruption[17]. On Ruapehu (New Zealand)[19] as on Bezymianny (Kamchatka)[20], the quasi-permanent high seismic activity of these volcanoes makes it difficult to clearly correlate timescales and seismicity. One recent study has used opx to decipher the processes and pre-eruptive conditions that led to the 1990 Kelud basaltic andesite eruption and showed a relationship between the timescales and the change of hydroacoustics and water lake temperature but the relationship with seismic swarms was more diffuse[18].

To conclude, at Kizimen, a magma mixing event occurred in the reservoir 1.5 years before the eruption, with a strong temporal correspondence to the onset of a seismic crisis. These correlations are a major feature of our findings and could help to identify future eruptions in case of a seismic reactivation not only on Kizimen but for future eruptions of volcanic systems involving differentiated magmas worldwide.

Materials And Methods

Sampling on the field: andesites, dacites and banded samples

Samples were collected in the pyroclastic deposits of the 2010–2013 eruption (Fig. 1a) during a three-week field mission which took place in August 2019. Samples coordinates can be found in **Supplementary Table 2**.

Sample preparation

The unaltered dacitic and andesitic samples were crushed (up to 3 mm). One half was then crushed again into fine powder for whole rock analysis while the other half was sieved into different size fractions (1 mm-710 µm, 710 – 500 µm, 500 – 355 µm, 355 – 250 µm, 250 – 125 µm). These fractions have been washed in ultrasonic bath and dried at 80°C for 48h. They were then observed under the binocular microscope to select the fractions in which the crystals were the more abundant and automorphic. Opx, plagioclase (plag), magnetites (mgt) and amphiboles (amph) were then handpicked under the binocular microscope in the different size fractions. They were mounted in epoxy resin and polished up to 0.3 µm to the middle part of the crystals. Opx were oriented with c-axis in a north-south direction as they have been used for intracrystalline diffusion modelling[19,25,55]. Before scanning electron microscope (SEM) or electron microprobe micro-analyzers (EPMA) investigations, selected mounts were all carbon-coated[55].

Textural observations: Scanning Electron Microscope

Opx were observed under Scanning Electron Microscopes (SEM): Zeiss Supra 55VP (Sorbonne Université, Institut des Sciences de la Terre de Paris, ISTeP, Paris) and the Carl Zeiss EVO MA10 SEM at the PARI platform at the Institut de physique du globe de Paris (Université de Paris) using an acceleration voltage of 20kV and a beam current of 8 nA. An identification of possible chemical zonations in the crystals (grey levels of different intensities) was possible in order to position the rim-core profiles to be carried out with the electron microprobe for opx. Proportions of zoned/unzoned opx crystals have been determined on all the crystals mounted by looking closely at the SEM images.

Higher resolution images (mag x755) were taken for the diffusion modelling and intercalibration with chemical profiles of opx with the same parameters as mentioned above, a high integration line (N = 7, 7 integrations of each image line to reduce the impact of noise) and a dwell time per pixel of 48 µs.

Compositional analysis of crystals

Whole rocks

Whole rock major-element compositions were analyzed by ICP-OES at Centre de Recherches Pétrographiques et Géochimiques (CRPG) in Nancy[56].

Point measurements

Opx crystals have been analysed for major elements (Si, Al, Ca, Mg, Na, K, Ti, Fe, Mn et P) by electron microprobe micro-analyzers with an acceleration voltage of 15 kV, a beam current of 10 nA and a focused beam of 2 µm (CAMECA SX-Five and SX-100; Service Camparis, Paris). Counting time on peak and

background for Fe and Mg was set at 80s and at 10s for the other elements. The core to rim compositional profiles in zoned opx had a 2 µm step and an average length of 100 µm (~ 4 hours per profile). Four points were measured across the unzoned crystals. They were acquired perpendicular to the long axes of the opx and away from the corners to avoid three-dimensional effects such as growth[28,55,57,58].

For compositional analyses in magnetite/ilmenite pairs to estimate the temperature, the counting time was set at 30s for Fe, Ti and Al and 10s for the other elements.

Timescales of magmatic processes

To investigate the changes in crystallization conditions in time and date the magmatic processes, interdiffusion timescales are modelled following the shapes of the concentration's profiles in opx and width of the diffusion zone between the plateaus. Using second Fick's law, if the initial conditions, boundary conditions and diffusion coefficient of the elements are known, fitting of the profiles can be used to obtain the timescales. The diffusion coefficient depends on parameters such as chemical composition (X_i; molar fraction of the mineral constituent element), temperature (T in Kelvin), pressure (P in Pa), oxygen fugacity (fO_2) and water fugacity (fH_2O)[6,7].

Modelling of the timescales associated to the zonations in the zoned crystals has been done by using the method developed in other studies[57,59], using the parametrization of the interdiffusion coefficient D of Fe and Mg elements in opx[60]. The Fe-Mg interdiffusion profiles were modelled in one dimension, across the c-axis, parallel to the b-axis of the crystals[57,59]. D depends on the composition of the opx, temperature, pressure, oxygen fugacity and water fugacity[6,25]. The interdiffusion coefficient we used here is formulated for a temperature between 500 and 800°C, an oxygen fugacity of IW + 0.8 log units above the IW buffer (IW: Iron-Wüstite buffer) and X_{Fe} ~ 0.10-0.50[60] (X_{Fe} is the molar fraction of the ferrosilite component). The parametrization of D in our model was done with a range of compositions of opx that includes those of this study (En_{44-73}; X_{Fe} = 0.23–0.53; **Supplementary Fig. 3**)[60], the temperature of the magmas are slightly above the range used in the parametrization of D, which is extrapolated at our temperatures. In the experimental study of D we used to model our timescales, they hypothesized an fO_2 dependence similar to olivine with an exponent of 1/6[60]. This fO_2 dependence has been incorporated in the formulation of D in other works[57,61] but this dependence has never been verified experimentally for opx with En contents of our dataset[62,63]. For En-rich opx of the mantle (En_{98} and En_{91}), between 870–1100°C and oxygen fugacity controlled ($fO_2 = 10^{-11}$-10^{-7} Pa), an fO_2 dependence of an exponent between 0 and 1/20 was found to be appropriate from their data[63]. The estimate for D_{Fe-Mg} used here[60], when extrapolated to higher temperatures of the study on En-rich opx without considering any fO_2 dependence appear to be consistent with their dataset[63]. The oxygen fugacity dependence on Fe-Mg interdiffusion coefficient is still under discussion as incorporating it can give longer timescales[47] but no study has yet examined the appropriate En compositions of the opx and appropriate oxygen fugacity

ranges. Therefore, the parametrization of the interdiffusion coefficient D used is the one determined on opx compositions close from our dataset without an fO_2 correction[60], as done in previous studies[25,55]. D is defined as follows in Eq. (1)[60]:

$$logD = -5.54 + 2.6\mathrm{X}_{Fe} - \frac{12530}{T} \# (1)$$

The main assumption of the model is that the initial profile between two zones follows a step function, which is modified by diffusion to form sigmoidal concentration gradients[64]. This steep profile becomes broader with time, due to interdiffusion of the different elements. With the eruption, the diffusion is stopped. Maximum timescales are then estimated[64]. Profiles with smooth compositional variations of sigmoid shape are studied and those displaying growth dominant profiles are isolated. These profiles display linear trends or curves and bumps on the profiles and are not consistent with a diffusion sigmoid calculated for the given initial compositional contrast[25] **(Supplementary Fig. 5**). The Al and Ca gradients are compared to the Mg#, as Al and Ca diffuse slower than Fe-Mg[47,57,65,66] (**Supplementary Data 1; Supplementary Fig. 5**).

The model that we used consists in the intercalibration of chemical composition profiles of zoned opx, measured with an electron microprobe, with grayscale profiles on high-resolution north-south oriented images taken with SEM (spatial resolution of 755 nm)[25,55], following the methodology developed in two other studies[57,59]. The Mg number is the parameter that seems to best control the grayscale of the images[50,59]. The *ImageJ* software (https://imagej.nih.gov/ij/; version 1.52a) is used to produce the grayscale profiles. They are averaged over a certain width to reduce the noise (between 20 to 50 µm, depending on the crystal rim size)[25,55]. After this intercalibration, the profiles are modelled to obtain the timescales of interdiffusion. As the diffusion coefficient used is composition-dependent, the curve shape of the profile is determined by the degree of compositional contrast but the curve width is dependent on time[25,59] Based on a library of profiles of particular values of compositional contrasts, the shape of the curve that fits the best to the one obtained by intercalibration will be searched in this library according to the compositional data[25]. The curve will then be scaled in width to solve for time and the timescale corresponding to the zonation is obtained, as the scaling factor is an expression of crystal composition, the diffusivity used for the library of the profiles, the diffusivity in the crystal and the ratio between the timescales of the database and the timescale associated with the zoning in the crystal[25] (with the timescale of the crystal being solved as the only unknown). The goodness of the fits is done by fitting the profiles by eye[25,55].

The determination of the temperature, the diffusion coefficient and its measurement are the main sources of uncertainties[6,64]. Uncertainties on the calibration of measurements and point spacing during EPMA analyses, as well as the resolution of SEM images are also sources of uncertainties (pixel size, uncertainty on grayscale values defining a plateau)[55]. Overall, the measurement of the diffusion coefficient and temperature represent the main sources of uncertainty and have a logarithmic effect on final calculated timescales[6,25,50] (**Supplementary Fig. 4**). Here, a Monte Carlo simulation was used to

estimate the integrated time uncertainty from the different sources of uncertainty (T, on D_0, E_a and resolution of grayscales values of SEM images), giving asymmetric uncertainties, with a larger error bar on the positive error and a smaller error bar on the negative error[25].

Estimation of earthquake magnitudes

The Kamchatka Branch of Russian Geophysical Survey uses the following magnitude M scale in Eq. (2):

$$M = log_{10}U + f\left(t_{S-P}\right) \# (2)$$

With $f\left(t_{S-P}\right)$ expressed in Eq. (3):

$$f\left(t_{S-P}\right) = \begin{cases} 1.42log_{10}\left(t_{S-P}\right) + 0.72, t_{S-P} < 7s \\ 2.44log_{10}\left(t_{S-P}\right) - 0.14, t_{S-P} \geq 7s \end{cases} \# (3)$$

where *U* is the maximum S-wave ground velocity in *micron/sec* and t_{S-P} is the arrival time difference between S and P waves. The seismic moments M_0 (in *N m*) are approximately estimated from magnitudes based on the moment magnitude equation in Eq. (4):

$$M_0 = 10^{(1.5M+9.05)} \# (4)$$

Declarations

Data and materials availability

Seismic catalog used for the analysis is available from the website of the Kamchatka Branch of the Geophysical Survey of Russian Academy of Sciences (http://sdis.emsd.ru/info/earthquakes/catalogue.php).

Acknowledgments

We would like to thank S. Hidalgo for her help with sample preparation, M. Fialin and N. Rividi for assistance during EPMA analyses, as well as O. Boudouma and S. Borensztajn for SEM imaging. We also thank D. M. for providing the files to model the timescales of the opx. We also acknowledge that the image from **Figure 1a** is from a Digital Elevation Model provided by the Polar Geospatial Center under NSF-OPP awards 1043681, 1559691, and 1542736 and **Figure 1b** from NASA Earth Observatory images by Robert Simmon, using Landsat 8 data from the USGS Earth Explorer. Thank you also to R. Bajou for the discussion on the cumulative number of earthquakes. This project was funded by the Institut de physique du globe de Paris (Doctoral grant from the French Ministry of Higher Education and Research and Innovation) and ANR V-Care-18-CE03-0010. The work of N.S., S.S., and S.D. has been supported by the Ministry of Science and Education of the Russian Federation under project no. 14.W03.31.0033 "Geophysical research, monitoring and forecasting of catastrophic geodynamic processes in the Russian Far East". The work of N.S. has been also supported by the European Research Council under the

European Union Horizon 2020 research and innovation program (Grant Agreement 787399-SEISMAZE). An open access license has been selected.

Author Contributions

L.O., H.B.B., G.B., A.B., M.B. and A.A. participated in the field mission in 2019 to collect the samples in Kamchatka (Russia). L.O. performed all data acquisition, prepared the figures and wrote the initial version of the manuscript during her PhD. L.O., H.B.B. and G.B. participated in the interpretation of the data and the writing of the manuscript text. N.S., S.S. and S.D. analyzed the seismic catalog of Kizimen and participated in the interpretation of the seismic data. All authors contributed to the writing of the manuscript text.

Competing Interest Statement

All the authors declare no competing interests.

References

1. Sparks, R. S. J. Forecasting volcanic eruptions. *Earth Planet. Sci. Lett.* **210**, 1–15 (2003).
2. Marti, J. *et al.* Correlation of Magma Evolution and Geophysical Monitoring during the 2011-2012 El Hierro (Canary Islands) Submarine Eruption. *J. Petrol.* **54**, 1349–1373 (2013).
3. Jay, J. *et al.* Locating magma reservoirs using InSAR and petrology before and during the 2011–2012 Cordón Caulle silicic eruption. *Earth Planet. Sci. Lett.* **395**, 254–266 (2014).
4. Caricchi, L., Biggs, J., Annen, C. & Ebmeier, S. The influence of cooling, crystallisation and re-melting on the interpretation of geodetic signals in volcanic systems. *Earth Planet. Sci. Lett.* **388**, 166–174 (2014).
5. McNutt, S. R. Seismic Monitoring and Eruption Forecasting of Volcanoes: A Review of the State-of-the-Art and Case Histories. in *Monitoring and Mitigation of Volcano Hazards* 99–146 (Springer Berlin Heidelberg, 1996). doi:10.1007/978-3-642-80087-0_3.
6. Costa, F. & Morgan, D. *Time Constraints from Chemical Equilibration in Magmatic Crystals*. *Timescales of Magmatic Processes: From Core to Atmosphere* (John Wiley & Sons, Ltd, 2010). doi:10.1002/9781444328509.ch7.
7. Costa, F., Shea, T. & Ubide, T. Diffusion chronometry and the timescales of magmatic processes. *Nat. Rev. Earth Environ.* **1**, 201–214 (2020).
8. Costa, F. Clocks in Magmatic Rocks. *Annu. Rev. Earth Planet. Sci.* **49**, 231–252 (2021).
9. Costa, F., Dohmen, R. & Chakraborty, S. Time Scales of Magmatic Processes from Modeling the Zoning Patterns of Crystals. *Rev. Mineral. Geochemistry* **69**, 545–594 (2008).
10. Mollo, S. & Hammer, J. E. Dynamic crystallization in magmas. in *Mineral reaction kinetics: Microstructures, textures, chemical and isotopic signatures* 378–418 (Mineralogical Society of Great Britain & Ireland, 2017). doi:10.1180/EMU-notes.16.12.

11. Chakraborty, S. Diffusion in Solid Silicates: A Tool to Track Timescales of Processes Comes of Age. *Annu. Rev. Earth Planet. Sci.* **36**, 153–190 (2008).
12. Morgan, D. J. *et al.* Magma chamber recharge at Vesuvius in the century prior to the eruption of A.D. 79. *Geology* **34**, 845 (2006).
13. Kahl, M., Chakraborty, S., Costa, F. & Pompilio, M. Dynamic plumbing system beneath volcanoes revealed by kinetic modeling, and the connection to monitoring data: An example from Mt. Etna. *Earth Planet. Sci. Lett.* **308**, 11–22 (2011).
14. Pankhurst, M. J., Morgan, D. J., Thordarson, T. & Loughlin, S. C. Magmatic crystal records in time, space, and process, causatively linked with volcanic unrest. *Earth Planet. Sci. Lett.* **493**, 231–241 (2018).
15. Kahl, M. *et al.* Compositionally zoned crystals and real-time degassing data reveal changes in magma transfer dynamics during the 2006 summit eruptive episodes of Mt. Etna. *Bull. Volcanol.* **75**, 692 (2013).
16. Rasmussen, D. J. *et al.* When does eruption run-up begin? Multidisciplinary insight from the 1999 eruption of Shishaldin volcano. *Earth Planet. Sci. Lett.* **486**, 1–14 (2018).
17. Saunders, K., Blundy, J., Dohmen, R. & Cashman, K. Linking Petrology and Seismology at an Active Volcano. *Science (80-.).* **336**, 1023–1027 (2012).
18. Utami, S. B., Costa, F., Lesage, P., Allard, P. & Humaida, H. Fluid fluxing and accumulation drive decadal and short-lived explosive basaltic andesite eruptions preceded by limited volcanic unrest. *J. Petrol.* **62**, 1–29 (2021).
19. Kilgour, G. N. *et al.* Timescales of magmatic processes at Ruapehu volcano from diffusion chronometry and their comparison to monitoring data. *J. Volcanol. Geotherm. Res.* **288**, 62–75 (2014).
20. Davydova, V. O., Shcherbakov, V. D. & Plechov, P. Y. The Timescales of Magma Mixing in the Plumbing System of Bezymianny Volcano (Kamchatka): Insights from Diffusion Chronometry. *Moscow Univ. Geol. Bull.* **73**, 444–450 (2018).
21. S.L. Senyukov, I. Nuzhdina, S. Droznina, V. Garbuzova, T. Kozhevnikova, O. S. Seismicity of Kizimen volcano. *Conf. Third Sci. Tech. Conf. 'Problems Integr. Geophys. Monit. Russ. Far East* (2011).
22. Dvigalo, V. N., Melekestsev, I. V., Shevchenko, A. V. & Svirid, I. Y. The 2010–2012 eruption of Kizimen Volcano: The greatest output (from the data of remote-sensing observations) for eruptions in Kamchatka in the early 21st century part I. The November 11, 2010 to December 11, 2011 phase. *J. Volcanol. Seismol.* **7**, 345–361 (2013).
23. Ji, L., Lu, Z., Dzurisin, D. & Senyukov, S. Pre-eruption deformation caused by dike intrusion beneath Kizimen volcano, Kamchatka, Russia, observed by InSAR. *J. Volcanol. Geotherm. Res.* **256**, 87–95 (2013).
24. Firstov, P. P. & Shakirova, A. A. Seismicity observed during the precursory process and the actual eruption of Kizimen Volcano, Kamchatka in 2009–2013. *J. Volcanol. Seismol.* **8**, 203–217 (2014).

25. Solaro, C. *et al.* A System Dynamics Approach to Understanding the deep Magma Plumbing System Beneath Dominica (Lesser Antilles). *Front. Earth Sci.* **8**, (2020).
26. Martel, C. *et al.* Effects of f O2 and H 2 O on andesite phase relations between 2 and 4 kbar. *J. Geophys. Res. Solid Earth* **104**, 29453–29470 (1999).
27. Metcalfe, A. *et al.* Magmatic Processes at La Soufrière de Guadeloupe: Insights From Crystal Studies and Diffusion Timescales for Eruption Onset. *Front. Earth Sci.* **9**, (2021).
28. Fabbro, G. N., Druitt, T. H. & Costa, F. Storage and Eruption of Silicic Magma across the Transition from Dominantly Effusive to Caldera-forming States at an Arc Volcano (Santorini, Greece). *J. Petrol.* **58**, 2429–2464 (2018).
29. Gorbatov, A., Kostoglodov, V., Suárez, G. & Gordeev, E. Seismicity and structure of the Kamchatka Subduction Zone. *J. Geophys. Res. Solid Earth* **102**, 17883–17898 (1997).
30. Park, J. *et al.* A Dangling Slab, Amplified Arc Volcanism, Mantle Flow and Seismic Anisotropy in the Kamchatka Plate Corner. in 295–324 (2002). doi:10.1029/GD030p0295.
31. Ponomareva, V. *et al.* Late Pleistocene-Holocene volcanism on the Kamchatka Peninsula, Northwest Pacific Region. in *Volcanism and Subduction: The Kamchatka Region* 165–198 (2007). doi:10.1029/172GM15.
32. Churikova, T., Dorendorf, F. & Wörner, G. Sources and Fluids in the Mantle Wedge below Kamchatka, Evidence from Across-arc Geochemical Variation. *J. Petrol.* **42**, 1567–1593 (2001).
33. Melekestsev, I. V., Ponomareva, V. V. & Volynets, O. N. Kizimen volcano, Kamchatka — A future Mount St. Helens? *J. Volcanol. Geotherm. Res.* **65**, 205–226 (1995).
34. Shapiro, N. M. *et al.* Deep and shallow long-period volcanic seismicity linked by fluid-pressure transfer. *Nat. Geosci.* **10**, 442–445 (2017).
35. Levin, V., Shapiro, N., Park, J. & Ritzwoller, M. Seismic evidence for catastrophic slab loss beneath Kamchatka. *Nature* **418**, 763–767 (2002).
36. Koulakov, I. *et al.* Mantle and Crustal Sources of Magmatic Activity of Klyuchevskoy and Surrounding Volcanoes in Kamchatka Inferred From Earthquake Tomography. *J. Geophys. Res. Solid Earth* **125**, (2020).
37. Melnik, O., Lyakhovsky, V., Shapiro, N. M., Galina, N. & Bergal-Kuvikas, O. Deep long period volcanic earthquakes generated by degassing of volatile-rich basaltic magmas. *Nat. Commun.* **11**, 3918 (2020).
38. Journeau, C. *et al.* Seismic tremor reveals active trans-crustal magmatic system beneath Kamchatka volcanoes. *Sci. Adv.* **8**, (2022).
39. Koulakov, I. *et al.* Three different types of plumbing system beneath the neighboring active volcanoes of Tolbachik, Bezymianny, and Klyuchevskoy in Kamchatka. *J. Geophys. Res. Solid Earth* **122**, 3852–3874 (2017).
40. Churikova, T., Wörner, G., Eichelberger, J. & Ivanov, B. Minor- and trace element zoning in plagioclase from Kizimen Volcano, Kamchatka: Insights on the magma chamber processes. in *Volcanism and*

Subduction: The Kamchatka Region 303–323 (2007). doi:10.1029/172GM22.

41. Auer, A., Belousov, A. & Belousova, M. Deposits, petrology and mechanism of the 2010–2013 eruption of Kizimen volcano in Kamchatka, Russia. *Bull. Volcanol.* **80**, 33 (2018).
42. Churikova, T. *et al.* Major and trace element zoning in plagioclase from Kizimen Volcano (Kamchatka): Insights into magma-chamber processes. *J. Volcanol. Seismol.* **7**, 112–130 (2013).
43. Girona, T., Costa, F., Newhall, C. & Taisne, B. On depressurization of volcanic magma reservoirs by passive degassing. *J. Geophys. Res. Solid Earth* **119**, 8667–8687 (2014).
44. Girona, T., Costa, F. & Schubert, G. Degassing during quiescence as a trigger of magma ascent and volcanic eruptions. *Sci. Rep.* **5**, 18212 (2015).
45. Tembrel, I. & Ovsyannikov, A. Activity of Kizimen volcano at summer 2009. *Bull Kamchatka Assoc Educ. Center. Earth Sci.* **14**, 7–9 (2009).
46. Sauerzapf, U., Lattard, D., Burchard, M. & Engelmann, R. The titanomagnetite-ilmenite equilibrium: New experimental data and thermo-oxybarometric application to the crystallization of basic to intermediate rocks. *J. Petrol.* **49**, 1161–1185 (2008).
47. Flaherty, T. *et al.* Multiple timescale constraints for high-flux magma chamber assembly prior to the Late Bronze Age eruption of Santorini (Greece). *Contrib. to Mineral. Petrol.* **173**, 75 (2018).
48. Kahl, M., Chakraborty, S., Pompilio, M. & Costa, F. Constraints on the Nature and Evolution of the Magma Plumbing System of Mt. Etna Volcano (1991–2008) from a Combined Thermodynamic and Kinetic Modelling of the Compositional Record of Minerals. *J. Petrol.* **56**, 2025–2068 (2015).
49. Kahl, M., Viccaro, M., Ubide, T., Morgan, D. J. & Dingwell, D. B. A Branched Magma Feeder System during the 1669 Eruption of Mt Etna: Evidence from a Time-integrated Study of Zoned Olivine Phenocryst Populations. *J. Petrol.* **58**, 443–472 (2017).
50. Solaro-Müller, C. Storage conditions and dynamics of magma reservoirs feeding the major pumiceous eruptions of Dominica (Lesser Antilles Arc). (University Paris Diderot, 2017).
51. Rae, A. S. P. *et al.* Time scales of magma transport and mixing at Kīlauea Volcano, Hawai'i. *Geology* **44**, 463–466 (2016).
52. Albert, H. *et al.* Magma interactions, crystal mush formation, timescales, and unrest during caldera collapse and lateral eruption at ocean island basaltic volcanoes (Piton de la Fournaise, La Réunion). *Earth Planet. Sci. Lett.* **515**, 187–199 (2019).
53. Longpre, M.-A., Klugel, A., Diehl, A. & Stix, J. Mixing in mantle magma reservoirs prior to and during the 2011-2012 eruption at El Hierro, Canary Islands. *Geol. Soc. Am. (GSA), Boulder, CO, United States* **42**, 315–318 (2014).
54. Ruth, D. C. S. *et al.* Crystal and melt inclusion timescales reveal the evolution of magma migration before eruption. *Nat. Commun.* **9**, 2657 (2018).
55. Ostorero, L. *et al.* Time - window into the transcrustal plumbing system dynamics of Dominica (Lesser Antilles). *Sci. Rep.* **11**, 1–15 (2021).

56. Carignan, J., Hild, P., Mevelle, G., Morel, J. & Yeghicheyan, D. Routine Analyses of Trace Elements in Geological Samples using Flow Injection and Low Pressure On-Line Liquid Chromatography Coupled to ICP-MS: A Study of Geochemical Reference Materials BR, DR-N, UB-N, AN-G and GH. *Geostand. Geoanalytical Res.* **25**, 187–198 (2001).
57. Allan, A. S. R., Morgan, D. J., Wilson, C. J. N. & Millet, M.-A. From mush to eruption in centuries: assembly of the super-sized Oruanui magma body. *Contrib. to Mineral. Petrol.* **166**, 143–164 (2013).
58. Krimer, D. & Costa, F. Evaluation of the effects of 3D diffusion, crystal geometry, and initial conditions on retrieved time-scales from Fe–Mg zoning in natural oriented orthopyroxene crystals. *Geochim. Cosmochim. Acta* **196**, 271–288 (2017).
59. Couperthwaite, F. K., Thordarson, T., Morgan, D. J., Harvey, J. & Wilson, M. Diffusion timescales of magmatic processes in the Moinui lava eruption at Mauna Loa, Hawai`i, as inferred from bimodal olivine populations. *J. Petrol.* **61**, 1–19 (2020).
60. Ganguly, J. & Tazzoli, V. Fe2+-Mg interdiffusion in orthopyroxene: retrieval from the data on intracrystalline exchange reaction. *Am. Mineral.* **79**, 930–937 (1994).
61. Allan, A. S. R. *et al.* A cascade of magmatic events during the assembly and eruption of a super-sized magma body. *Contrib. to Mineral. Petrol.* **172**, 49 (2017).
62. Stimpfl, M., Ganguly, J. & Molin, G. Kinetics of Fe2+–Mg order–disorder in orthopyroxene: experimental studies and applications to cooling rates of rocks. *Contrib. to Mineral. Petrol.* **150**, 319–334 (2005).
63. Dohmen, R., Ter heege, J. H., Becker, H.-W. & Chakraborty, S. Fe-Mg interdiffusion in orthopyroxene. *Am. Mineral.* **101**, 2210–2221 (2016).
64. Morgan, D. J. *et al.* Time scales of crystal residence and magma chamber volume from modelling of diffusion profiles in phenocrysts: Vesuvius 1944. *Earth Planet. Sci. Lett.* **222**, 933–946 (2004).
65. Smith, D. & Barron, B. R. Pyroxene-garnet equilibration during cooling in the mantle. *Am. Mineral.* **76**, 1950–1963 (1991).
66. Cherniak, D. J. & Dimanov, A. Diffusion in Pyroxene, Mica and Amphibole. *Rev. Mineral. Geochemistry* **72**, 641–690 (2010).
67. Minster, J. B. & Jordan, T. H. Present-day plate motions. *J. Geophys. Res.* **83**, 5331 (1978).
68. Konstantinovskaia, E. . Arc–continent collision and subduction reversal in the Cenozoic evolution of the Northwest Pacific: an example from Kamchatka (NE Russia). *Tectonophysics* **333**, 75–94 (2001).
69. Porter, Claire; Morin, Paul; Howat, Ian; Noh, Myoung-Jon; Bates, Brian; Peterman, Kenneth; Keesey, Scott; Schlenk, Matthew; Gardiner, Judith; Tomko, Karen; Willis, Michael; Kelleher, Cole; Cloutier, Michael; Husby, Eric; Foga, Steven; Nakamura, Hitomi; Pl, M. *"ArcticDEM"*. (2018) doi:https://doi.org/10.7910/DVN/OHHUKH.
70. Portnyagin, M. & Manea, V. C. Mantle temperature control on composition of arc magmas along the Central Kamchatka Depression. *Geology* **36**, 519 (2008).

71. Viccaro, M., Giuffrida, M., Nicotra, E. & Ozerov, A. Y. Magma storage, ascent and recharge history prior to the 1991 eruption at Avachinsky Volcano, Kamchatka, Russia: Inferences on the plumbing system geometry. *Lithos* **140–141**, 11–24 (2012).

Figures

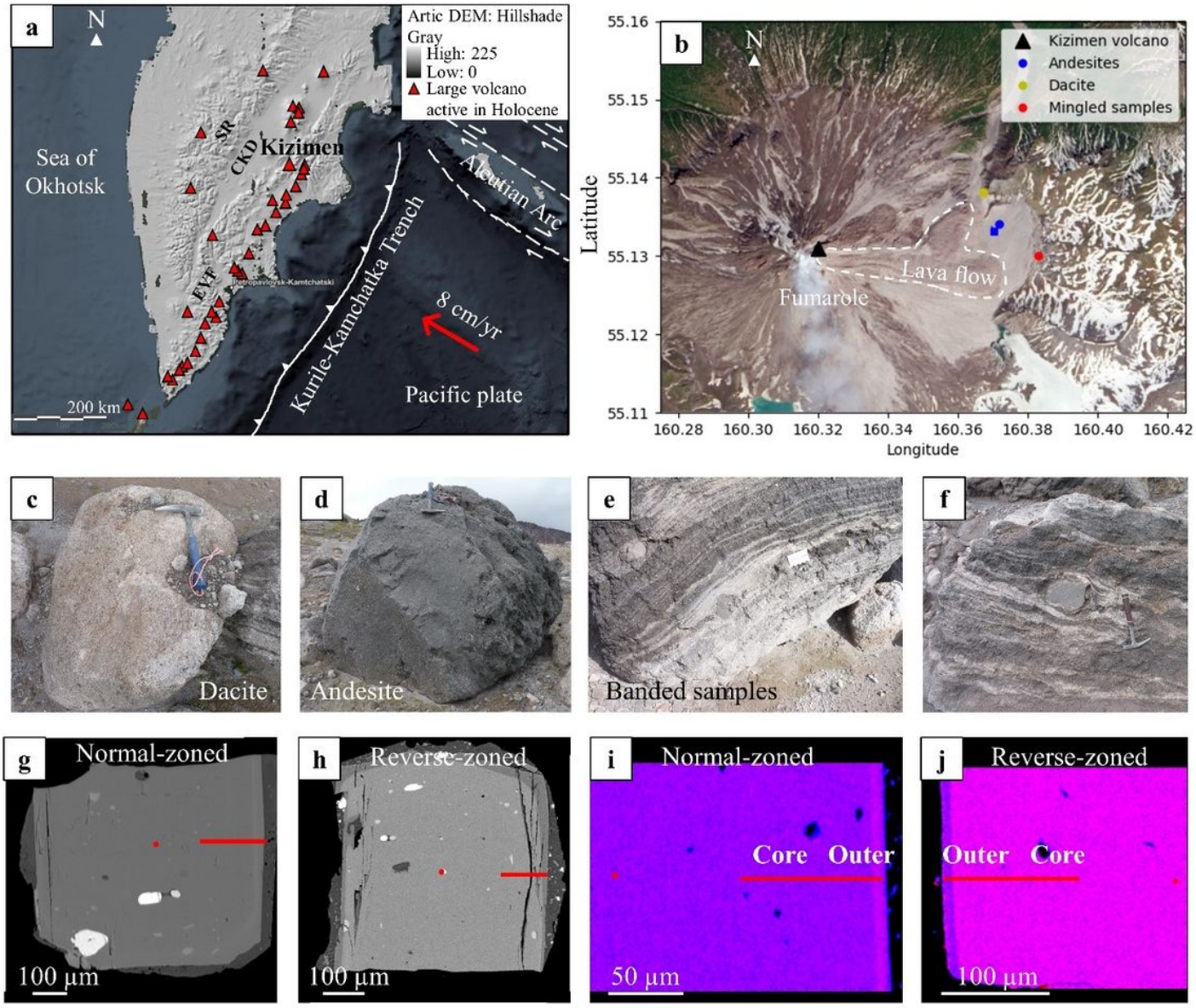

Figure 1

From macroscale to microscale: Kizimen location in Kamchatka, 2010-2013 eruption samples and opx zonations. a) Kamchatka map with the three volcanic zones: Sredinny Range (SR), Central Kamchatka Depression (CKD) and Eastern Volcanic Front (EVF)[32,33] and the boundary of the active subduction zone of the Kurile-Kamchatka Trench (subduction rate of 8 cm/yr[29,67,68]). Image from the ArticDEM: Hillshade Gray from the ArcGIS Living Atlas of the World (by Esri Imagery, courtesy of the Polar Geospatial Center;

https://livingatlas2.arcgis.com/arcticdemexplorer/)[69] and modified according to other studies[70,71]. **b)** Sampling sites on Kizimen (**Supplementary Table 2**) (Image credit: Nasa Earth Observatory image from June 17, 2014, using Landsat 8 data from the United States Geological Survey (USGS) Earth Explorer; courtesy of Robert Simmon). **c)** Dacite (64 wt% SiO_2; 5.6 wt% Na_2O +K_2O). **d)** Andesite (58-60 wt% SiO_2; 4.8-5 wt% Na_2O +K_2O). **e-f)** Banded samples (alternation between dacitic and andesitic bands[41]). **g-h)** Major zonations identified in the dacite and andesite: normal and reverse zonations, respectively. **i)** Red-Green-Blue (RGB) chemical map of a normal-zoned opx, with a Mg-rich core (darker in color than the rims) and Fe-rich rims ("Outer" on (**i-j**)). **j)** Reverse-zoned opx, with a Fe-rich core and Mg-rich rims.

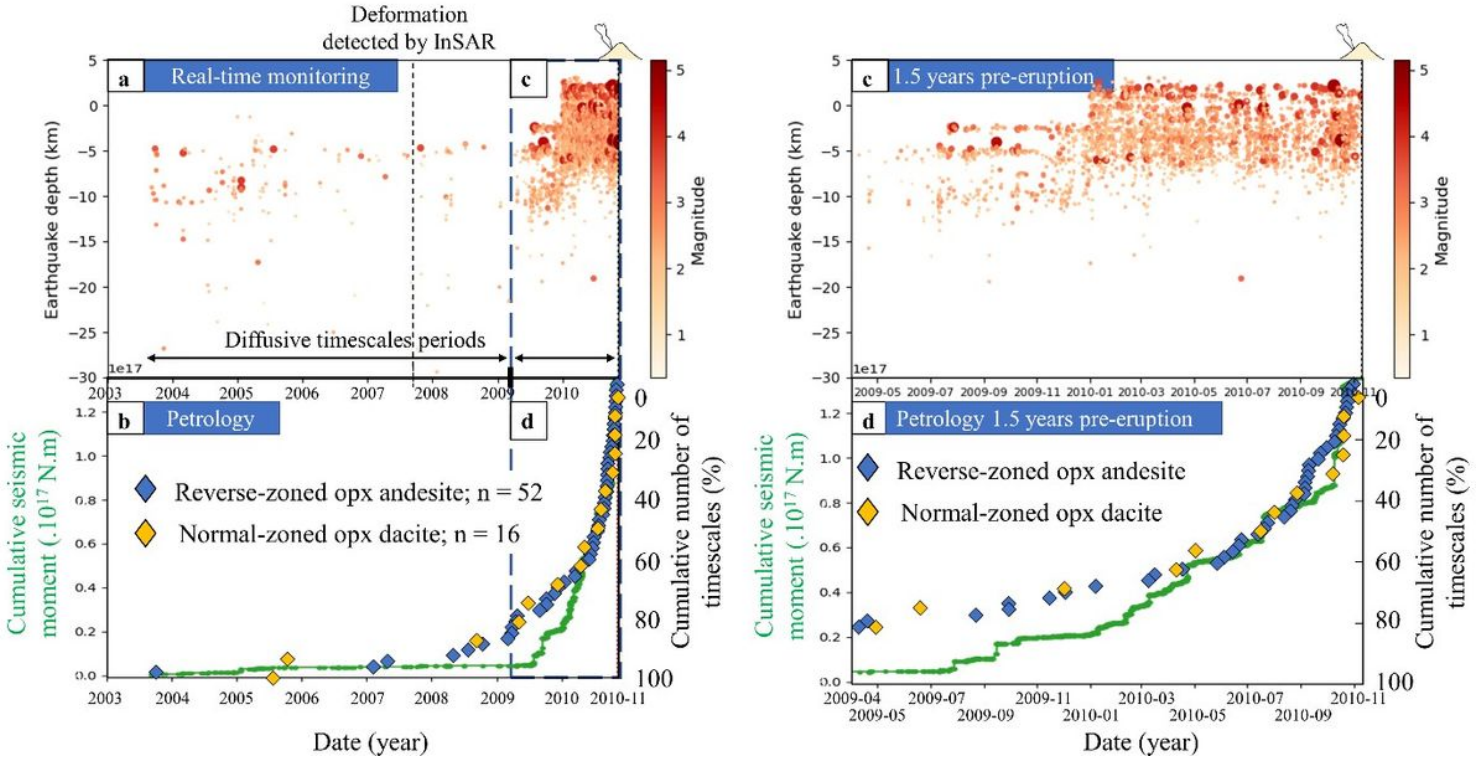

Figure 2

Linking monitoring data with timescales estimations of magmatic processes. a) Time vs depth plot of seismicity at Kizimen from 2003 to the onset of the eruption (11/11/2010)[21,41]. The onset of the surface deformation detected by InSAR is specified[23,41]. **b)** Cumulative number of the timescales estimated on the major compositional changes evidenced for the dacite and andesite (normal zoning for the dacite (En_{62-64} to En_{44-54}) and reverse zoning for the andesite (En_{62-64} to En_{64-73}); **Supplementary Data 3**) and cumulative seismic moment. **c)** and **d)** Focus on the 1.5 years pre-eruption.

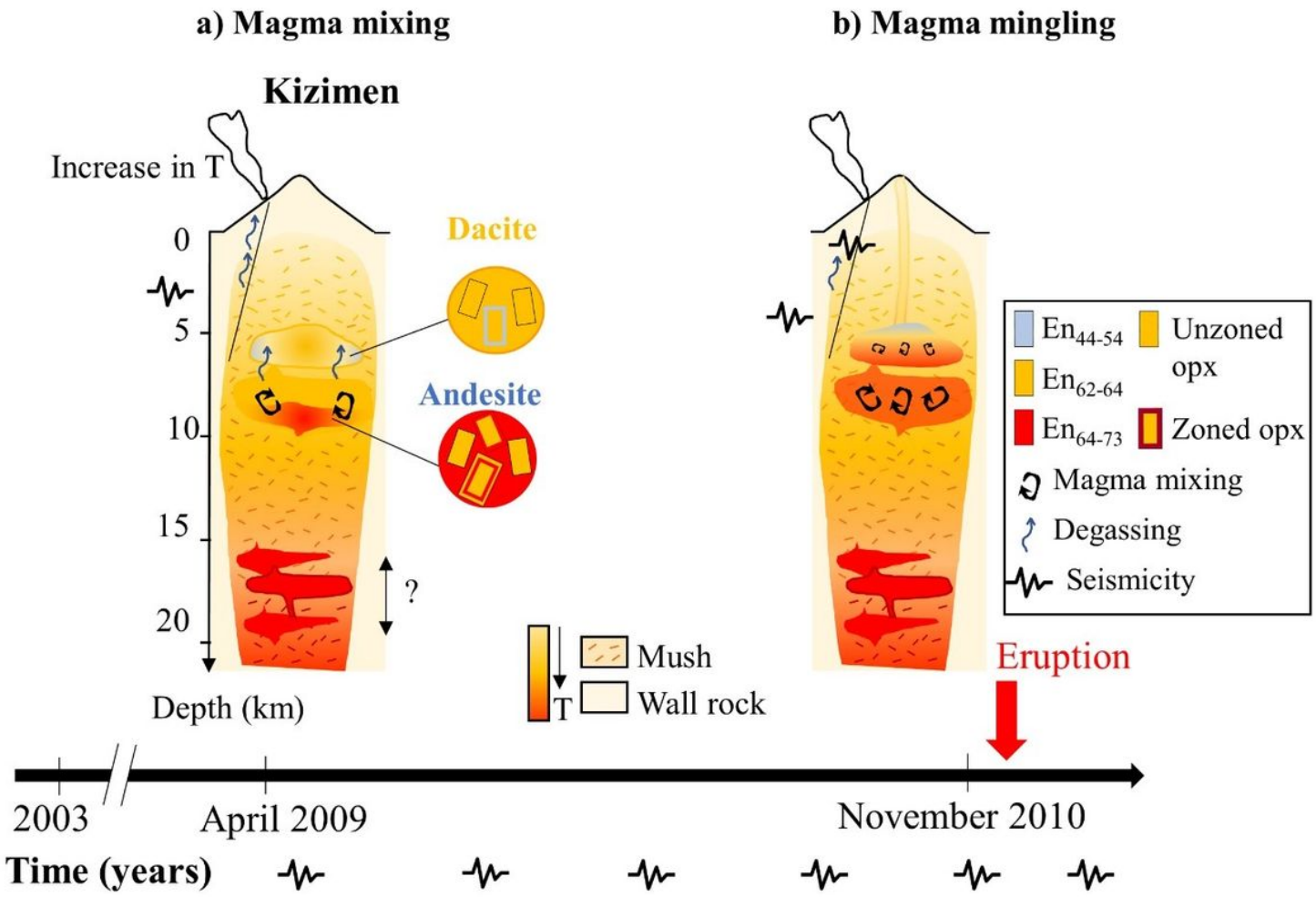

Figure 3

Pre-eruptive dynamics of the magmas in the timeframe given by the timescales modelled in zoned opx: 1.5 years before the eruption. a) Magma mixing in the lower zoned reservoir between the walls and center of the reservoir occurring 1.5 years before the eruption, forming the reverse-zoned opx, by increase of the temperature (*T*). The architecture of the plumbing system of a previous study was used[41]: a dacitic reservoir which has been intruded by a basaltic injection in 1963[21,24,41], with the lower part of the dacitic reservoir becoming andesitic by hybridization with the mafic magma. This mixing event also affected the upper dacitic part of the reservoir with some degassing processes due to the saturation of the fluid phase[15], forming normal-zoned opx, as well as the seismicity recorded during this period. Not all the reservoir was affected by the mixing as there is a majority of unzoned opx. The deeper part of the trans-crustal system may be composed of mafic lenses. **b)** Then, magma mingling occurred between andesitic and dacitic lower parts, shortly before the eruption. The dacitic and andesitic reservoir have the same mineral assemblage: plagioclase, opx, amphiboles, Fe-Ti oxides and some resorbed olivines and quartz (*T* = 832 ± 37°C and 847 ± 57°C, respectively).

Supplementary Files

This is a list of supplementary files associated with this preprint. Click to download.

- SIKizimenTimescales.pdf
- SupplementaryData1.xlsx
- SupplementaryData2.xlsx
- SupplementaryData3.xlsx